Journal of Materials Chemistry B

PAPER

View Article Online
View Journal | View Issue



Cite this: J. Mater. Chem. B, 2015, 3, 9360

# Structure-solubility relationships in fluoride-containing phosphate based bioactive glasses

Yaqoot Shaharyar,[ab] Eric Wein,[a] Jung-Ju Kim,[cd] Randall E. Youngman,[e] Francisco Muñoz,[f] Hae-Won Kim,[cdg] Antonio Tilocca[h] and Ashutosh Goel*[a]

The dissolution of fluoride-containing bioactive glasses critically affects their biomedical applications. Most commercial fluoride-releasing bioactive glasses have been designed in the soda–lime–silica system. However, their relatively slow chemical dissolution and the adverse effect of fluoride on their bioactivity are stimulating the study of alternative biodegradable materials with higher biodegradability, such as bio-degradable phosphate-based bioactive glasses, which can be a good candidate for applications where a fast release of active ions is sought. In order to design new biomaterials with controlled degradability and high bioactivity, it is essential to understand the connection between chemical composition, molecular structure, and solubility in physiological fluids. Accordingly, in this work we have combined the strengths of various experimental techniques with Molecular Dynamics (MD) simulations, to elucidate the impact of fluoride ions on the structure and chemical dissolution of bioactive phosphate glasses in the system: $10Na_2O–(45 - x)CaO–45P_2O_5–xCaF_2$, where $x$ varies between 0–10 mol%. NMR and MD data reveal that the medium-range atomic-scale structure of these glasses is dominated by $Q^2$ phosphate units followed by $Q^1$ units, and the MD simulations further show that fluoride tends to associate with network modifier cations to form alkali/alkaline-earth rich ionic aggregates. The impact of fluoride on chemical dissolution of glasses has been studied in deionized water, acidic (pH = 3.0), neutral (pH = 7.4) and basic (pH = 9.0) buffer solutions, while the bioactivity and cytotoxicity of glasses has been studied *in vitro* through their apatite-forming ability in simulated body fluid (SBF) and cell culture tests on mesenchymal stem cells (MSCs), respectively. The macroscopic trends observed from various chemical dissolution and bioactivity studies are discussed on the basis of the effect of fluoride on the atomistic structure of glasses, such as F-induced phosphate network re-polymerization, in an attempt to establish composition–structure–property relationships for these biomaterials.

Received 24th July 2015,
Accepted 11th November 2015

DOI: 10.1039/c5tb01494h

www.rsc.org/MaterialsB

## 1. Introduction

Fluoride-releasing biomaterials have found wide application in the field of dentistry due to their anticariogenic properties,[1] ability to control enamel demineralization[2] and treat dentine hypersensitivity.[3] Today, there are several commercial fluoride-containing dental restoratives where fluorinated glasses are an integral component, for example, glass-ionomers and resin modified glass ionomer cements. As the majority of these materials are silicate-based glass systems, substantial effort has been made to unearth the underlying structural drivers that control the bioactivity of fluoride containing silicate glasses.[4–7] However, the major drawback of silicate- based glass systems, and in particular of fluoride-containing phosphosilicate glasses, is their slow chemical degradation, often requiring long times – months to years – to completely disappear from the body.[8,9] Fluoride is known as "corrosion inhibitor" in silicate glasses[10] as it tends to increase the polymerization of silicate tetrahedra by removing modifiers from the siliceous matrix.[4] Therefore, non-silicate completely bioresorbable glass systems are being explored as potential third generation biomaterials.[11]

Bioactive glasses designed in the polyphosphate region of the $Na_2O–CaO–P_2O_5$ system are an ideal example of

[a] Department of Materials Science and Engineering, Rutgers, The State University of New Jersey, Piscataway, NJ, 08854, USA. E-mail: ashutosh.goel@rutgers.edu; Tel: +1-848-445-4512
[b] Department of Chemical Engineering, Rutgers, The State University of New Jersey, Piscataway, NJ, 08854, USA
[c] Institute of Tissue Regeneration Engineering (ITREN), Dankook University, Cheonan 330-714, South Korea
[d] Department of Nanobiomedical Science & BK21 PLUS NBM Global Research Center for Regenerative Medicine, Dankook University, Cheonan 330-714, South Korea
[e] Science and Technology Division, Corning Incorporated, Corning, NY 14831, USA
[f] Ceramics and Glass Institute (CSIC), Kelsen 5, 28049 Madrid, Spain
[g] Department of Biomaterials Science, School of Dentistry, Dankook University, Cheonan 330-714, South Korea
[h] Department of Chemistry, University College London, 20 Gordon Street, London WC1H 0AJ, UK

bioresorbable materials. In particular, the glass composition system: $(Na_2O)_{55-x}(CaO)_x(P_2O_5)_{45}$ (where $x$ varies between 30–45 mol%) has received considerable attention owing to its favorable attributes such as controlled chemical dissolution, good cyto-compatibility, along with its soluble nature.[12–15] According to Bitar *et al.*,[16] glasses with CaO content lower than 40 mol% support little or no cell adhesion and survival due to their high solubility which does not allow cell adhesion to the labile glass surface (as has also been shown by Gough *et al.*).[17,18] On the other hand, glass compositions with CaO content varying between 40–48 mol% have been shown to up-regulate human osteoblast cell lines and certain antigens, including bone sialoprotein and fibronectin, which play a major role in maintaining the structure and integrity of bone.[17,18] A substantial effort has also been made towards understanding the influence of dopants ($Cu^{2+}$, $Ag^{+}$ and $Ti^{4+}$) on the bioactivity of these glasses.[11,19] However, studies describing the influence of fluoride incorporation on structure, and properties of phosphate based bioactive glasses are scarce.

In the case of fluorinated phosphate glasses, several studies have focused on describing the structural role of fluoride in alkali phosphate,[20] tin phosphate,[21] and aluminophosphate glass systems.[22] It has been reported that fluoride depolymerizes the chain structure of $NaPO_3$ by replacing bridging P–O–P bonds with terminal P–F species. In the case of fluoride containing aluminophosphate glasses, several authors reported that F is predominantly bonded to Al rather than P,[22–24] and almost no P–F bonds were detected in Na–Al–P–O–F glasses by $^{19}F$ NMR.[25] Although the results obtained in these studies represent valid reference points for understanding the influence of fluoride on the phosphate glass structure, they cannot be straightforwardly translated to bioactive glass systems due to significant differences in their glass chemistry. The influence of fluoride on the structure of phosphate-based bioactive glasses in the system $20Na_2O–30CaO–50P_2O_5$ has been recently investigated using *ab initio* molecular dynamics (AIMD).[26] Based on a substantial amount of F–P bonding found in the AIMD models, it was proposed that the glass network could be structurally homogeneous on medium-range length scales. However, in this specific case the necessarily small number of fluorine atoms in the *ab initio* model, in connection with the slow convergence of the P–F coordination number (discussed below), may interfere with the accurate evaluation of P–F bonding based on the AIMD data alone. Larger MD samples and/or corresponding experimental data are thus needed for a full assessment of the effect of fluoride on the phosphate glass structure.

In the light of the above mentioned perspective, the present study is focused on understanding the impact of fluoride incorporation on the structure, solubility and *in vitro* bioactivity of soda lime phosphate glasses. Based on the existing literature in this domain, we have chosen a $10Na_2O–45CaO–45P_2O_5$ (mol%) composition as a model glass system where CaO has been substituted by $CaF_2$ in the range of 0–10 mol%. An attempt has been made to combine the strengths of various experimental techniques with molecular dynamics (MD) simulations,[27,28] to elucidate the impact of fluoride ions on the structure–property relationships in bioactive phosphate glasses.

# 2. Experimental and computational techniques

## 2.1 Glass synthesis

The high-purity powders of $NH_4H_2PO_4$ (99%, Alfa Aesar), $Na_2CO_3$ (99%, FMC Corporation), $CaCO_3$ (99%, Alfa Aesar) and $CaF_2$ (99%, Alfa Aesar) were used to prepare batches. Homogeneous mixtures of batches ($\sim$50 g), were melted in pure platinum crucibles (covered with a Pt–Rh lid) at 1100 °C for 1 h in air. Glass frits were obtained by quenching the melt in cold water followed by drying. The glasses have been labeled in accordance with their respective $CaF_2$ content, *i.e.* F-0, F-2.5, F-5, F-7.5, and F-10. The amorphous nature of glasses was confirmed by X-ray diffraction (XRD) analysis (PANalytical – X'Pert Pro; Cu $K_\alpha$ radiation; $2\theta$ range: 10°–90°; step size: 0.007° $s^{-1}$). The dried glass frit was crushed in a planetary ball mill (Fritsch PULVERISETTE 6 classic line) to obtain glass powders with particle size range varying between 300–425 μm and $<$120 μm, respectively.

## 2.2 Structural characterization

**2.2.1 Thermal stability.** The thermal stability of glasses was studied by differential thermal analysis (DTA, STA8000, Perkin Elmer Inc.). The glass powders (particle size $<$120 μm) weighing $\sim$50 mg were contained in an alumina pan and scanned in air from 30 °C to 1000 °C at a heating rate ($\beta$) of 20 K $min^{-1}$. The glass transition temperature ($T_g$), onset of crystallization ($T_c$), peak temperature of crystallization ($T_p$) and melting temperature ($T_m$) were obtained from the DTA thermographs of all the glasses.

**2.2.2 Magic angle spinning – nuclear magnetic resonance (MAS-NMR).** $^{31}P$ MAS NMR experiments were conducted at 11.7 T (202.3 MHz resonance frequency) using a commercial spectrometer (VNMRs, Agilent) and 3.2 mm MAS NMR probe (Varian/Chemagnetics). Powdered glasses were packed into 3.2 mm zirconia rotors with sample spinning at 20 kHz. Radio frequency pulses (0.6 μs), corresponding to a $\pi/6$ tip angle, were used along with a 60 s recycle delay to collect nominally 1000 acquisitions. The $^{31}P$ MAS NMR spectra were processed with minimal Gaussian line broadening (25–50 Hz) and frequency (shift) referenced to 85% $H_3PO_4$ at 0 ppm. The spectra were fit with Gaussian lineshapes, using commercial software (Grams), and all spinning sidebands were taken into account while determining the $Q^n$ speciation.

$^{23}Na$ MAS and triple quantum MAS (3QMAS) NMR experiments were conducted at 16.4 T (185.12 MHz resonance frequency) using a commercial spectrometer (VNMRs, Agilent) and 1.6 mm MAS NMR probe (Agilent). Powdered glasses were packed into 1.6 mm zirconia rotors, with MAS spinning frequencies of 30 kHz. Short RF pulses (0.6 μs $\approx$ $\pi/12$ tip angle) to uniformly excite the $^{23}Na$ resonances, along with a 1 second recycle delay, were used to acquire 1000 transients, which were subsequently processed without apodization and frequency referenced to aqueous NaCl at 0 ppm. $^{23}Na$ 3QMAS NMR experiments were performed using the hyper-complex shifted-echo pulse sequence.[39] RF pulses were calibrated to provide optimized signal to-noise ratio, resulting in hard pulse widths of 2.6 and 1.0 μs, and a soft $z$-filter reading pulse of 10 μs. 240 acquisitions

were collected for each of 40 $t_1$ values. These data were processed with 50 Hz apodization in both time domains and referenced to aqueous NaCl at 0 ppm. Average $\delta_{iso}$ and $C_q$ values for sodium in these glasses were calculated from the 3QMAS NMR spectra using the procedures described by Amoureux *et al.*[29]

**2.2.3 Molecular dynamics simulations.** Classical molecular dynamics (MD) simulations with the DL_POLY code[30] were performed to obtain atomic-scale models of the glasses, using a well-established computational framework for modeling bioactive glasses.[31–33] The force field employed here is based on the shell-model (SM) potential for bioactive phosphosilicate glasses developed by Tilocca *et al.*,[33–35] where full ionic charges are employed. Oxygen atoms are represented as core–shell units connected by damped harmonic springs; Buckingham terms describe the interactions between oxygen shells (Os) with each other and with P, Na, and Ca, using the potential parameters previously reported.[36] The additional Buckingham parameters for the interaction of $F^-$ ions with each other and with Os, P, Na and Ca ions were fitted to the crystalline structures of fluoroapatite, difluorophosphoric acid anhydride, NaF, and $CaF_2$. Finally, a three-body truncated harmonic potential is used to control the intra-tetrahedral Os–P–Os angle within phosphate groups, but no arbitrary constraints (such as P–O–P angle terms) are placed on the inter-tetrahedral structure.

Three compositions ($x$ = 0, 5, 10 in $(45 - x)$ CaO–$10Na_2O$–$45P_2O_5$–$xCaF_2$) were modeled. For each composition, the simulation was started from a completely random initial configuration containing approximately 3000 atoms; the two fluorinated compositions modeled, $x$ = 5 and 10, contained 68 and 136 fluorine atoms, respectively. This starting configuration was inserted in a periodic cubic box of ~35 Å side, yielding a density corresponding to the experimental one or, when no experimental data were available, to the one estimated based on the measured effect of CaO → $CaF_2$ substitution on the density of Na–Ca silicate bioglasses.[37] The system was then heated and equilibrated at 2500 K for 60 ps, and then continuously cooled to room temperature at a cooling rate of 5 K $ps^{-1}$. The latter rate has been recently shown to produce MD models of melt-derived bioactive glasses with a sufficiently accurate medium-range structure.[38] A final 200 ps MD run at room temperature was then performed to produce the reference trajectory employed for the structural analysis reported below.

### 2.3 Apatite forming ability of glasses in simulated body fluid (SBF)

The apatite forming ability of glasses was investigated by immersion of glass powders (<120 μm) in SBF (0.1 g glass powder in 50 ml SBF solution) at 37 °C. SBF had an ionic concentration ($Na^+$ 142.0, $K^+$ 5.0, $Ca^{2+}$ 2.5, $Mg^{2+}$ 1.5, $Cl^-$ 125.0, $HPO_4^-$ 1.0, $HCO_3^{2-}$ 27.0, $SO_4^{2-}$ 0.5 mmol $l^{-1}$) nearly equivalent to human plasma, as discussed by Tas.[39] The powder–SBF mixtures were immediately sealed into sterilized plastic flasks and were placed in an oven at 37 °C. The SBF solution was replaced every 48 h and sampling took place at different times varying between 1 h and 5 days. The experiments were performed in duplicate in order to ensure the accuracy of results. The apatite forming ability on glass powders was followed by XRD and Fourier transform infrared (FTIR) spectroscopy. The IR spectra were acquired using a universal attenuated total reflectance sensor (FTIR-UATR, Frontier™, Perkin Elmer Inc.; scanning resolution: 4 $cm^{-1}$, 32 scans for background and samples). Raman spectra were measured using a Renishaw inVia Raman microscopes with a 785 nm wavelength laser, operating at 500 mW. Eight acquisitions were taken for each scan. The reference spectra of hydroxyapatite and fluorapatite minerals were obtained from the online RRUFF project database of Department of Geosciences, The University of Arizona. The elemental release profile of glasses in SBF during initial 48 h was measured using inductive coupled plasma – optical emission spectroscopy (ICP-OES; Optima 8× series, Perkin Elmer Inc.) while pH evolution in SBF was followed using a pH meter (SevenCompact™ S230, Mettler Toledo Inc.).

### 2.4 Chemical dissolution of glasses in deionized water

The chemical dissolution of glass powders (<120 μm) in Type II deionized (DI) water (pH: 5.50) was investigated by immersing 0.1 g glass powder in 50 ml DI water at 37 °C. The powder–water mixtures were immediately sealed into sterilized plastic flasks and were placed in an oven at 37 °C. The dissolution experiments were performed in the time duration varying between 1 h to 7 days. All the experiments were performed in duplicate in order to ensure the accuracy of results. The changes in glass structure pre- and post-dissolution were followed by XRD and FTIR-UATR. The elemental release profile of glasses in DI water was measured using ICP-OES while pH evolution in DI water was followed using a pH meter.

### 2.5 Physico-chemical degradation of glasses in accordance with ISO-10993-14

The degradation tests were performed according to the standard ISO 10993-14 "Biological evaluation of medical devices – Part 14: identification and quantification of degradation products from ceramics". The test comprises two parts. The first part of the test deals with investigating the degradation behavior of glasses/ceramics in citric acid buffer solution with pH = 3.0. The choice of citric acid solution has been made since osteoclasts release this acid while an extreme low pH = 3.0 simulates a worst case low-end environment. The second part of the test simulates a more frequently encountered *in vivo* pH (7.4 ± 0.1) and therefore investigates the degradation of glasses/ceramics in freshly prepared tris-HCl buffered solution. In order to understand the influence of pH on the chemical degradation of glasses, we have also studied the chemical degradation of glasses in tris-HCl at pH = 9. In accordance with ISO standard, 5 g glass powder with particle size varying between 300–425 μm was immersed in 100 ml solution at 37 °C for 120 h. The sampling was done after duration of 120 h where the solid and liquid phases were separated by filtering (0.22 μm, Millex GP, Millipore Corporation, U.S.A). The solid samples were then washed in DI water and dried in an oven to constant weight. The pH along with elemental release profile of glasses in different buffer

 

solutions was measured. A relative weight loss percentage of glass samples after 120 h of immersion in solutions were calculated from the pre- and post-dissolution weight of glass powders while the structural changes in glasses were followed by XRD and FTIR.

### 2.6 *In vitro* cell culture studies

Mesenchymal stem cells (MSCs) derived from rat bone marrow were used to study the *in vitro* cell responses to the as developed glasses. Cells were maintained in a normal culture medium containing α-minimal essential medium (MEM) supplemented with 10% fetal bovine serum (FBS), 100 U $ml^{-1}$ penicillin and 100 mg $ml^{-1}$ streptomycin in a humidified atmosphere of 5% $CO_2$ in air at 37 °C. The glasses were sterilized with 70% ethanol for 1 h and then oven-dried prior to seeding cells. The cell responses were analyzed by means of an indirect test. For this, cells were seeded at $1 \times 10^4$ in each well of 12-well plates and then allowed to adhere to the surface for 4 h. After this, the transwell insert (Corning, cat no. 353182) containing each glass sample (F-0, F-5 and F-10; dimensions: $8 \times 8 \times 5$ $mm^3$) was placed on the culture well, and then incubated for predetermined culture periods.

For the cell viability assay, the cell morphology was first observed using an optical microscopy. The quantification of cell viability was also carried out by a cell counting kit assay (CCK-8). In brief, at the culture period of 2 and 5 days, 500 μl of CCK-kit solution mixture was poured into each sample, and then incubated at 37 °C for 3 h, after which 100 μl of the reaction medium was transferred to 96-well plate and then the optical density at 450 nm was measured by microplate reader (BioRad).

The osteogenic differentiation of the MSCs was analyzed by determining the alkaline phosphatase (ALP) activity of cells. Cell culture medium contained additional osteogenic factors (50 μg ascorbic acid, 10 mM β-glycerophosphate, and 100 nM dexamethasone). After culture for 10 days, the MSCs were disrupted through alternating cycles of freezing and thawing step, and then 0.2% triton X-100 was treated for 3 h at 4 °C. The cell pallets were gathered by a centrifugation. For an enzymatic reaction, the supernatant solution was added to the 100 μl of ALP reaction medium according to the manufacturer's instructions (Sigma). After 1 h of incubation at 37 °C, 100 μl of stop solution was added and then the absorbance of the eluted yellow product was measured at 415 nm using microplate reader (BioRad). The measured values were normalized to the ds DNA content.

The CCK and ALP assays were carried out in triplicate, and statistical analysis was carried out by one-way ANOVA for $n = 3$. Significance was considered at $p < 0.05$, and $p < 0.01$.

## 3. Results

### 3.1 Glass forming ability

Homogeneous, XRD amorphous glasses were obtained from compositions with $CaF_2$ content varying between 0–10 mol%. We tried to synthesize a glass with 12.5 mol% $CaF_2$ content, but did not succeed as the melt was highly prone to phase separation/crystallization, resulting in white colored opaque frit even on quenching in cold water. A thin layer of white colored precipitates on the bottom part of the Pt–Rh lid (covering the Pt crucible) was observed after melting of fluorinated glasses, implying towards the volatilization of fluorine from glass melts. Although we did not quantify the experimental glass compositions, fluorine loss from these glasses cannot be neglected. According to the literature, 5–23% $CaF_2$ is lost from fluoride-containing phosphosilicate glasses during melting.[40] We could not obtain a similar reference data point for fluoride solubility/retention in phosphate glass melts.

The presence of fluorine in glasses was indirectly confirmed by the thermal analysis of the studied glasses. Fig. 1 presents the DTA thermographs of glasses F-5 and F-10 at heating rate of 20 K $min^{-1}$ as the representative scans for the glasses investigated in the present study, while Table 1 presents the values of thermal parameters obtained for all the glasses. The glass transition temperature ($T_g$) remained almost constant (469.5 ± 0.47 °C) with increasing $CaF_2$ concentration in glasses from 0 to 7.5 mol%. The addition of 10 mol% $CaF_2$ in glass F-10 led to an increase in its $T_g$ to ~480 °C. The phenomenon of glass transition was followed by onset of crystallization ($T_c$) that tends to shift gradually towards lower temperatures with increasing $CaF_2$ content until glass F-7.5. The value of $T_c$ moved towards higher temperature by 10 °C in glass F-10 (in comparison to glass F-7.5) as is evident from Table 1. The crystallization was represented by a single exothermic curve (following $T_c$) for glasses with $CaF_2$ content varying between 0–5 mol%. The peak temperature of crystallization ($T_{p1}$) shifted towards lower temperatures with increasing $CaF_2$ content in glasses. A broad shoulder could be observed in the crystallization curves of glasses F-7.5 and F-10, indicating the formation of two-or more crystalline phases in

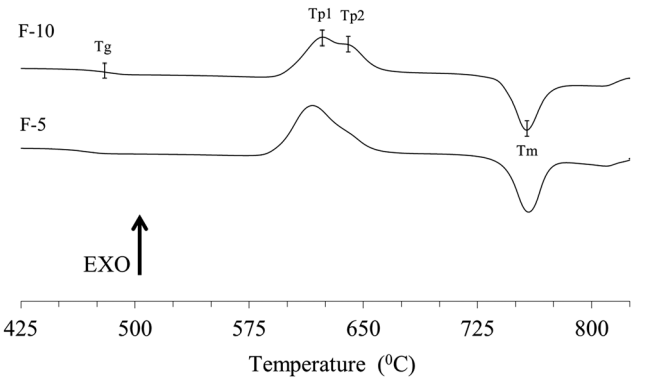


Fig. 1 DTA thermographs of glasses F-5 and F-10 at 20 K $min^{-1}$ in air.

Table 1 Thermal parameters as obtained from DTA

| Glass | $T_g$ | $T_{c1}$ | $T_{p1}$ | $T_{p2}$ | $T_m$ | $K_H$ |
|---|---|---|---|---|---|---|
| F-0 | 470 | 608 | 637 | — | 760 | 1.13 |
| F-2.5 | 470 | 609 | 636 | — | 759 | 1.12 |
| F-5 | 469 | 595 | 619 | — | 759 | 0.90 |
| F-7.5 | 470 | 591 | 611 | 638 | 759 | 0.82 |
| F-10 | 480 | 600 | 623 | 638 | 757 | 0.90 |

these glasses with increasing fluoride content. In coherence with the trend observed for $T_g$ and $T_c$, the value of $T_{p1}$ for glass F-10 shifted towards higher temperature in comparison to glass F-7.5 while no such variation was observed in $T_{p2}$ values. The crystallization was followed by a sharp endothermic event ($T_m$) at 759 ± 1.1 °C in all the glasses corresponding to melting of crystalline phases.

$$K_H = \frac{T_c - T_g}{T_m - T_c} \quad (1)$$

Hrubý parameter was calculated for all the glasses using eqn (1). According to Hrubý,[41] the larger value of $K_H$ implies towards greater stability against crystallization on heating and, presumably, greater vitrifiability on cooling. The values of $K_H$ tend to decrease with increasing $CaF_2$ content in glasses until 7.5 mol% indicating the decreasing thermal stability of glasses with fluoride incorporation. A higher $K_H$ value pointing towards higher thermal stability was obtained for glass F-10 (in comparison to F-7.5).

### 3.2 Structural characterization of glasses

**3.2.1 MAS-NMR results.** Short-range structure in these glasses was investigated with $^{31}P$ and $^{23}Na$ NMR spectroscopy. The phosphate speciation, as reflected in the $^{31}P$ MAS NMR data in Fig. 2a, consists entirely of $Q^1$ and $Q^2$ polyhedra, corresponding to the resonances at −9 ppm and −25 ppm, respectively. Integration of the peak intensities, including all associated spinning sidebands (not shown), allows for accurately quantification of the phosphate groups (Table 2). The data in Fig. 2a, as well as the fitting results in Table 2, indicate little change in phosphate groups with incorporation of $CaF_2$. The only noticeable difference in $Q^1$ and $Q^2$ populations is for glass F-10, which contains a slightly higher fraction of $Q^2$ groups.

$^{23}Na$ NMR studies were also made to ascertain the bonding environment of sodium, especially as a function of added fluoride. $^{23}Na$ MAS NMR spectra are plotted in Fig. 2b, showing a single, broad line-shape for all glasses. The position of this resonance under MAS NMR is a combination of both the

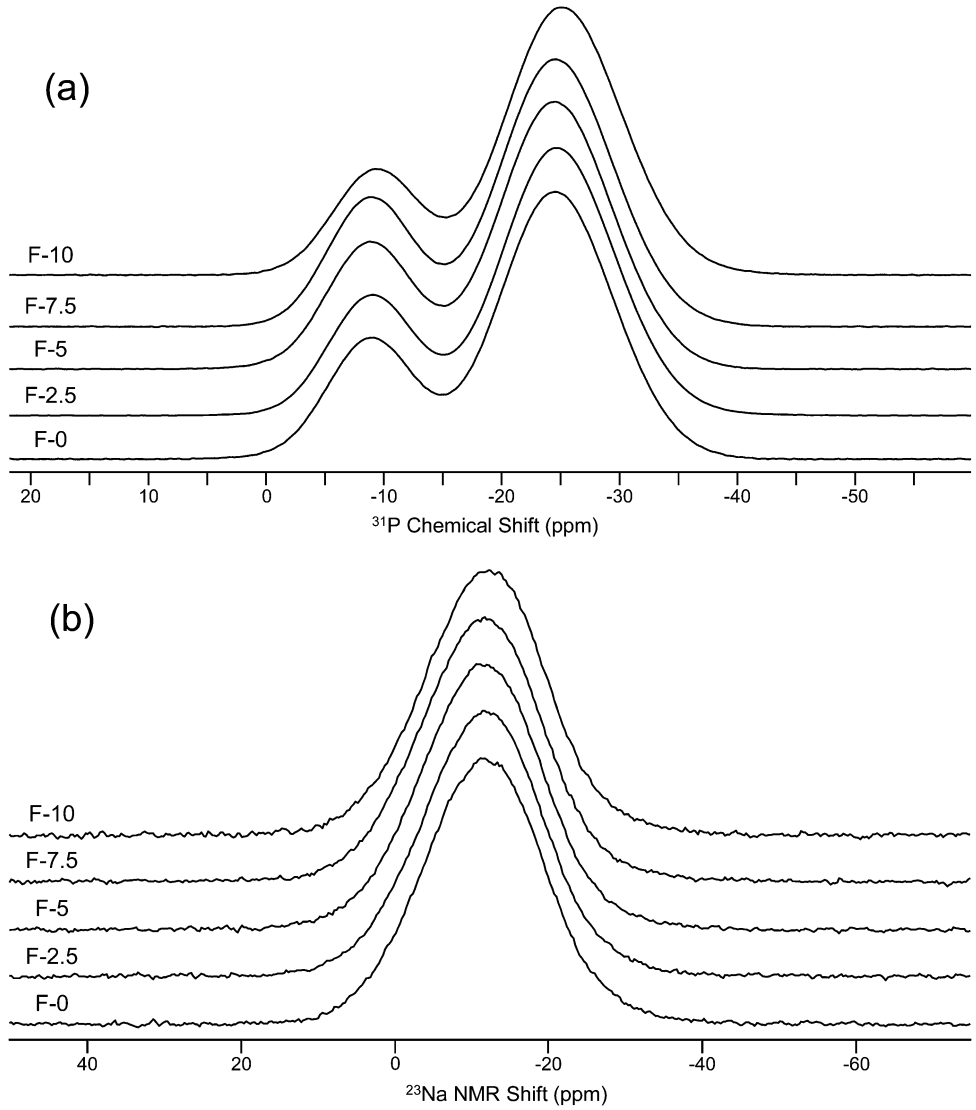


Fig. 2 (a) $^{31}P$ MAS NMR and (b) $^{23}Na$ MAS NMR spectra for this series of glasses.

 

Table 2 NMR results based on $^{31}$P MAS NMR and $^{23}$Na 3QMAS NMR spectroscopy. $^{31}$P peak areas included all spinning sidebands. $^{23}$Na NMR parameters extracted using peak position in the isotropic and MAS dimensions, as described by Amoureaux *et al.*[40]

| | $^{31}$P | | | | $^{23}$Na | |
|---|---|---|---|---|---|---|
| | $Q^1$ | | $Q^2$ | | | |
| Glass | $\delta_{CS}$ (ppm) (±0.1) | Population (%) (±1) | $\delta_{CS}$ (ppm) (±0.1) | Population (%) (±1) | $\delta_{iso}$ (ppm) (±1) | $P_Q$ (MHz) (±0.2) |
| F-0 | −8.9 | 22 | −24.8 | 78 | −6.2 | 2.8 |
| F-2.5 | −8.9 | 22 | −24.8 | 78 | −5.9 | 2.8 |
| F-5 | −8.8 | 23 | −24.7 | 77 | −6.1 | 2.7 |
| F-7.5 | −8.8 | 24 | −24.7 | 76 | −6.5 | 2.6 |
| F-10 | −9.2 | 20 | −25.3 | 80 | −6.9 | 2.6 |

$^{23}$Na chemical shift and a 2nd-order quadrupolar induced shift from the spin-3/2 nucleus. Even without direct determination of the $^{23}$Na chemical shifts in these spectra, it is apparent that addition of $CaF_2$ does not appear to affect the sodium environment in these glasses, as the peaks in Fig. 2b are nearly identical for all glasses. $^{23}$Na 3QMAS NMR data were also collected to determine chemical shift and quadrupolar coupling values for sodium. The spectra (Fig. 3) were analyzed using the position of the $^{23}$Na resonance in both frequency dimensions to calculate the $^{23}$Na isotropic chemical shift ($\delta_{iso}$) and quadrupolar coupling product ($P_Q$), using the methods of Amoureaux *et al.*[29] These values are included in Table 2, confirming very little change in either parameter for the sodium in these glasses.

**3.2.2 Analysis of MD simulations.** The radial distribution functions (rdfs) in Fig. 4 confirm the accuracy of the force field employed here. The P–O rdf for the F-free composition shows a main peak split into two subpeaks at 1.51 and 1.61 Å, corresponding to P=O and P–O bonds, in agreement with high-energy XRD data for similar compositions.[42] The peaks of the Ca–O, Na–O and O–O rdfs are found at 2.34, 2.37 and 2.56 Å, respectively, also in good agreement with the experimental data. The figure also shows that no marked changes occur in these distances upon $CaF_2$ incorporation, which therefore does not appear to affect the short-range (local) structure of these glasses. The top panel of the figure shows the rdfs pertaining to

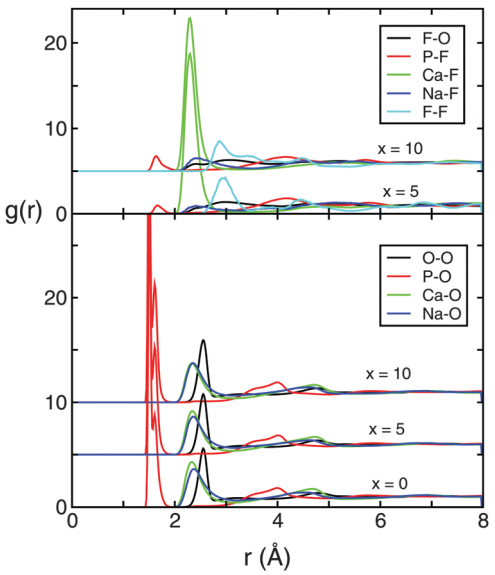


Fig. 4 Radial distribution functions obtained from the MD simulations for pair interactions involving oxygen (bottom panel) and fluorine (top panel).

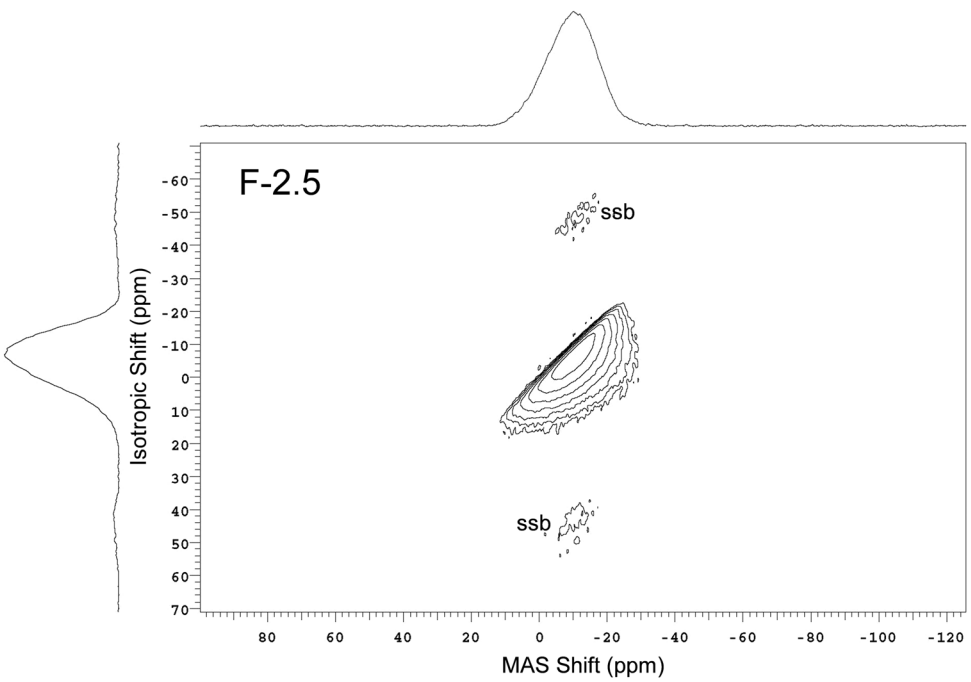


Fig. 3 $^{23}$Na 3QMAS NMR spectrum of F-2.5 glass. Isotropic and MAS projections are shown to the left and top of the two-dimensional plot. Contours belong to spinning sidebands are denoted by ssb. Extraction of $\delta_{iso}$ and $P_Q$ from the peak positions are described in the text.

Table 3 A–B (B–A) coordination numbers, obtained by integrating the relevant radial distribution functions (rdfs) obtained from MD simulations, up to the indicated cutoff distance $R_c$ (Å) corresponding to the first rdf minimum

| | P–O (O–P) | P–F (F–P) | Na–O (O–Na) | Na–F (F–Na) | Ca–O (O–Ca) | Ca–F (F–Ca) |
|---|---|---|---|---|---|---|
| $X$ | $R_c$ = 2.0 | $R_c$ = 2.0 | $R_c$ = 3.15 | $R_c$ = 3.35 | $R_c$ = 3.15 | $R_c$ = 3.25 |
| 0 | 4.0 (1.28) | NA | 6.68 (1.03) | NA | 6.42 (1.47) | NA |
| 5 | 3.99 (1.30) | 0.01 (0.11) | 6.27 (0.45) | 0.10 (0.21) | 5.83 (0.95) | 0.61 (2.76) |
| 10 | 3.96 (1.32) | 0.04 (0.20) | 6.18 (0.46) | 0.3 (0.3) | 5.33 (0.89) | 1.13 (2.55) |

fluoride in the two simulated fluorinated compositions. Peaks corresponding to P–F (1.63 Å), Ca–F (2.29 Å), Na–F (2.40 Å), O–F and F–F (2.9–3.0 Å) distances, in absence of relevant experimental data, could be compared to distances measured in previous AIMD simulations of fluorinated phosphate and P-containing bioglasses,[26,43] which yielded corresponding values of 1.58, 2.2–2.25, 2.3 and 3 Å. The agreement is again rather good, taking into account that the different composition and the corresponding different local environment surrounding fluoride ions are known to markedly affect the F-related distances.[44]

Table 3 shows the coordination numbers (CNs) obtained from the MD models. The main message of these data is that, at least up to $x$ = 10, fluoride is predominantly (although not exclusively) associated to Na and Ca. Only a relatively small amount of fluorine atoms bond to phosphorus, but this P–F bonded fraction appears to increase with increasing $CaF_2$ fraction: 10% and 20% of all F atoms are bonded to P for $x$ = 5 and 10, respectively. The total number of (O + F) atoms bonded to P remains four, indicating that bonding to F does not affect the tetrahedral coordination of phosphorus. It is important to note that the amount of P–F bonding in the melt is initially much higher and only converges slowly to its equilibrium value during the heating/cooling phase. This seems to denote that exceedingly fast cooling rates relative to the already considerably fast standard values used in MD simulations[38] may prevent the full convergence of this key property for these systems.

Regarding the association to modifier cations, a much higher number of fluoride ions are found in the coordination shell of Ca than Na: this was also evident from the sharp peak in the Ca–F rdfs in Fig. 4 as opposed to the much smaller Na–F peak. Table 4 shows the $Q^n$ distribution determined from the MD models of the three compositions. The distribution obtained for the F-free parent composition (F-0) is closer to the NMR data obtained in this work for the same composition, the main difference being the small $Q^3$ fraction in the model which was not detected by NMR. This distribution is also well compatible with the results previously obtained for related F-free phosphate bioactive glasses using classical MD.[45] The substitution of $CaF_2$ for CaO leads to a re-polymerization of the phosphate network, as indicated by a decrease in $Q^1$ and corresponding increase in $Q^2$ and $Q^3$ species, reflected in the ~8% increase in network connectivity as $x$ increases from 0 to 10 (Table 4). The NMR data also highlighted a possible network re-polymerization, but only starting for the highest ($x$ = 10) $CaF_2$ fraction, which could be interpreted based on the loss of fluoride content due to volatilization during melting of the experimental glasses (which does not occur in the simulations) that shifts these trends to higher fluoride contents.

Table 4 $Q^n$ distribution determined from the MD models of the three compositions. NC is the corresponding network connectivity

| $X$ | $Q^0$ | $Q^1$ | $Q^2$ | $Q^3$ | $Q^4$ | NC |
|---|---|---|---|---|---|---|
| 0 | 0.08 | 26.6 | 68.9 | 4.4 | 0 | 1.78 |
| 5 | 0.58 | 19.25 | 73.25 | 6.9 | 0 | 1.87 |
| 10 | 0.61 | 13.5 | 77.8 | 8.0 | 0.05 | 1.93 |

Based on these results, the main effect of fluoride incorporation in these compositions appears to be the removal of modifier cations, especially Ca, from the phosphate network, promoting its re-polymerization. Because the amount of P–F bonding appears to be enhanced with increasing $CaF_2$ amount, further studies would be needed to understand whether the above re-polymerization effect may change at higher fluoride levels.

### 3.3 *In vitro* bioactivity of glasses

**3.3.1 Apatite forming ability of glasses in SBF.** Fig. 5a shows the XRD patterns of glass powders demonstrating their amorphous nature prior to their immersion in SBF solution, while the FTIR spectra of all the glass powders are presented in Fig. 5b. All the investigated glasses show five broad bands in 400–1600 $cm^{-1}$ region. The broadness clearly shows the disorder in the glass structure with uneven distribution of $Q^n$ units ($Q$ is the degree of polymerization and $n$ is the number of bridging oxygens). The band centered at ~475 $cm^{-1}$ corresponds to the deformation modes of $PO_2$ units, while the band at 1260 $cm^{-1}$ can be attributed to the asymmetric stretching of $PO_2$ terminal groups.[46] Similarly, the bands ~750 $cm^{-1}$ and 890 $cm^{-1}$ can be assigned to the symmetric vibrations of bridging oxygens in P–O–P bonds[46] and, asymmetric stretching modes of P–O–P linkages,[47] respectively while, the transmittance band at ~1094 $cm^{-1}$ can be assigned to $P–O^-$ (chain terminator) groups.[47]

The immersion of glass powders in SBF for 1 h resulted in the formation of crystalline phases on the surface of these glasses as is evident from their XRD and FTIR data shown in Fig. 6a and b, respectively. Since the results obtained by soaking glass powders in SBF for prolonged durations were similar to those obtained after 1 h, we have focused our analysis and discussion on the results obtained from 1 h of glass–SBF interaction.

The XRD data of glass powders after dissolution in SBF for 1 h demonstrates the formation of calcium phosphate apatite along with aragonite ($CaCO_3$) as shown in Fig. 6a. The FTIR

 

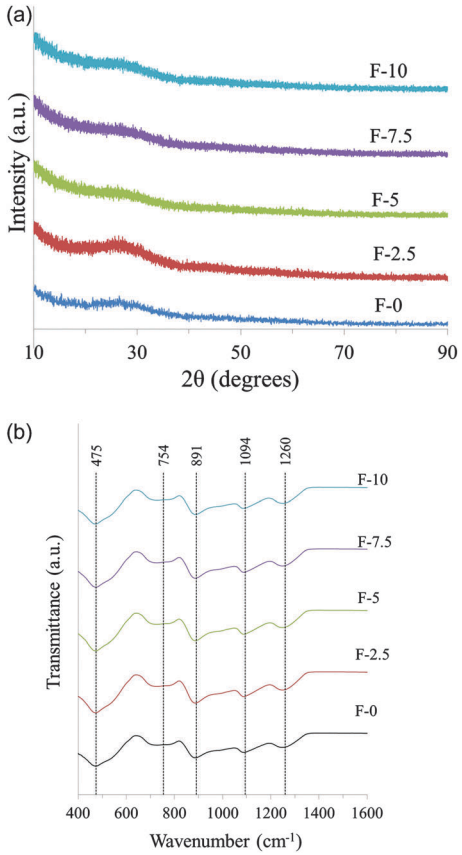


Fig. 5 (a) XRD data of parent glasses depicting their amorphous nature, (b) FTIR spectra of glass powders.

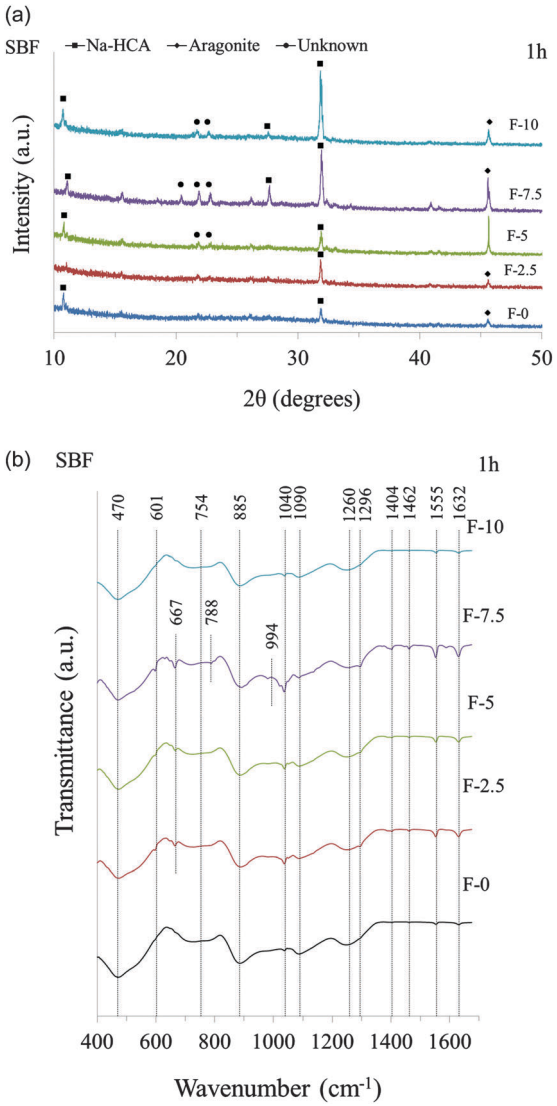


Fig. 6 (a) X-ray diffraction patterns, and (b) FTIR spectra of glasses after immersion in SBF for 1 h.

spectra of glass powders (Fig. 6b) are in good agreement with XRD data as sharp signature bands for calcium phosphate apatite (1040, 1090, 601, and 470 $cm^{-1}$) and carbonates (1555, 1462 and 1404 $cm^{-1}$)[48] can be observed for all the glasses. Our analysis of XRD data yielded three different apatite minerals *i.e.* stoichiometric hydroxyapatite [$Ca_5(PO_4)_3OH$; PDF#97-005-0656; hereafter referred as HAp], sodium-doped carbonated hydroxyapatite [$Ca_{8.8}Na_{1.2}(PO_4)_{4.8}(CO_3)_{1.2}(CO_3)$; PDF#97-015-3906; hereafter referred as Na-HCA] and fluorapatite [$Ca_5(PO_4)_3F$; PDF#97-003-4228; hereafter referred as FAp] as the best possible matches. The possibility of the presence of stoichiometric HAp was negated as the phase reflection corresponding to 100% intensity for this crystal structure appears at $2\theta = 25.85^\circ$ which does not match with our experimental data ($2\theta = 31.85^\circ$, $I = 100\%$). The phase reflections for Na-HCA and FAp demonstrate a good fit with the experimental data. However, the most intense peaks for these phases almost overlap each other at $2\theta = 31.85^\circ$ (Na-HCA) and 31.93 (FAp), thus making it difficult to ascertain the presence of any one phase. Therefore, Raman spectroscopy was employed to differentiate between the Na-HCA *vs.* FAp. According to literature, $\nu_3$ phosphate vibration mode of HAp is located at 959–962 $cm^{-1}$,[49] whereas in FAp it is slightly shifted towards 965–966 $cm^{-1}$.[50] In this study, the Raman spectra of all the samples (after immersion in SBF for 1 h) were completely masked by fluorescence (as shown in Fig. 7) due to which we could not observe any signature bands for HAp or FAp (in the 960–965 $cm^{-1}$ region) as reported in literature. It should be noted that fluorescence is often observed in Raman spectra of apatite samples, especially when the specimens are studied in powdered form.[51,52] Therefore, we used the Raman spectra of hydroxyapatite and fluorapatite minerals (obtained using an un-polarized laser) overwhelmed with fluorescence as reference spectra. As shown in Fig. 7, only the broad band of the reference HAp at ~1330 $cm^{-1}$ tends to overlap with the major band obtained in the glass samples under investigation, while no other band observed in the studied glasses overlaps with the reference patterns. Whereas this does not allow us to confirm the exclusive presence of either HCA or FAp in the samples under investigation, our interpretation – in combination with the other data – is that the apatite formed on these glasses comprises a mixture of both Na-HCA and FAp in different proportions as a function of fluoride content in glasses.

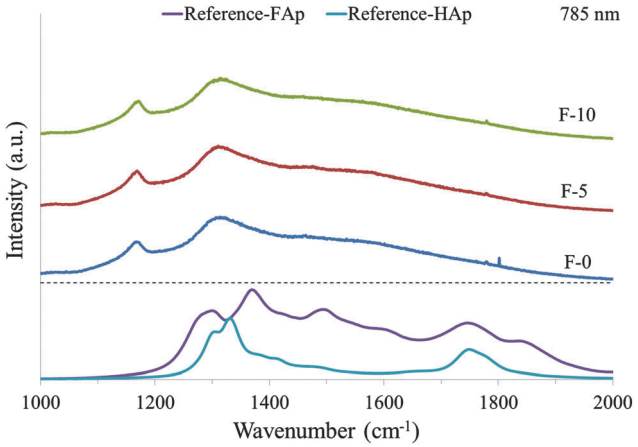


Fig. 7 Raman spectra of glass powders F-0, F-5 and F-10 (after immersion in SBF for 1 h) at 785 nm with 500 mW power unpolarized laser. Reference spectra for unoriented samples of hydroxylapatite ($Ca_{5.00}(P_{1.00})O_4)_3((OH)_{0.98}Cl_{0.02}$) and fluorapatite ($Ca_{5.00}((P_{0.98}Si_{0.02})O_4)3F_{1.00}$) at 780 nm@100% of 600 mW pump power.

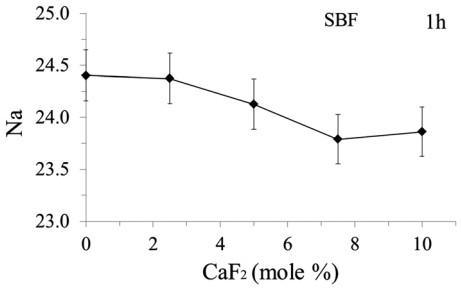


Fig. 8 Normalized sodium release rate from glass powders (with respect to their $CaF_2$ content) after 1 hour of dissolution in SBF.

With regard to the carbonate substitution in hydroxyapatite, the characteristic FTIR peaks for A-type HCA (hydroxyl is substituted by carbonate group) are known to appear at 880, 1450 and 1540 $cm^{-1}$ while that for B-type HCA (phosphate group is substituted by carbonate group) appear at 870, 1430 and 1450 $cm^{-1}$.[53] In our study, the characteristic band at ~1550 $cm^{-1}$ has been used to confirm the presence of A-type HCA. The FTIR band at ~1462 $cm^{-1}$ may be attributed to aragonite[54] while 1630 $cm^{-1}$ band represents adsorbed molecular $H_2O$. Since most of the characteristic IR bands for A-type and B-type HCA tend to overlap each other, it is difficult to negate the possibility of mixture of both A/B-type HCA. According to literature, B-type is the preferential carbonate substitution found in the bone of a variety of species, with A/B type ratio in the range 0.7–0.9.[55]

Soda-lime phosphate glasses are known to dissolve congruently in aqueous media through a two-step process: (1) hydration reaction where the glass exchanges its $Na^+$ with $H^+$ ions from the aqueous solution to carry out the formation of a hydrated layer on the glass surface; (2) network breakage where $H^+$ ions and molecular water attack the P–O–P bonds in hydrated layer resulting in destruction of the glass network and leading to the release of phosphate chains with different degree of polymerization into the aqueous solution,[56–58] a mechanism not dissimilar to that established for silicate bioglasses.[59] Because of the moisture adsorption on the glass surface during its preparation and storage period, P–O–P breakage takes place inside the hydrated layer formed before the dissolution process. Once in contact with SBF, the short chain polyphosphates or orthophosphates quickly dissolve into aqueous solution, leading to rapid increase of phosphate concentration in SBF. On the other hand, while SBF is already calcium and phosphate rich, the affinity of phosphate chains in SBF to chelate with divalent calcium attracts the latter from the hydrated layer of glass into SBF resulting in deposition of apatite and calcium carbonate phases on the glass network structure.[56,60] The deposition of crystalline phases acts as a protective film over the hydrated layer preventing further diffusion of molecular water into the bulk glass.[56]

When compared with fluorinated silicate bioactive glasses,[5,7,61] we did not find any significant influence of fluoride on apatite forming ability of phosphate-based bioactive glasses as apatite and aragonite phases were observed in all the glasses after 1 h of immersion in SBF and the same crystalline phase assemblage was maintained over the period of 120 h. However, fluoride incorporation in phosphate glasses does affect their initial chemical dissolution (before significant network breakage takes place, step 2) as can be seen in the normalized sodium release profile of glasses (with respect to $CaF_2$ content) in SBF after 1 h immersion (Fig. 7). We focused only on the sodium release profile because the dissolution of phosphate glasses is initiated by $Na^+ \leftrightarrow H^+$ ion exchange. It has been shown in literature that $Ca^{2+} \leftrightarrow H^+$ ion exchange reaction does not occur during the formation of the hydrated layer at the glass–water interface.[56] As is evident from Fig. 8, increasing $CaF_2$ content in glasses led to a slight decrease in their sodium release rate during the first hour of dissolution in SBF. Prolonged duration tests (for example: 48 h) reveal that sodium concentration in SBF was almost the same for all the glasses irrespective of the fluoride content suggesting the dominance of step 2 (network breakage) in glass dissolution.

**3.3.2 *In vitro* cell culture studies.** The effect of fluoride release from glasses on the cell viability in culture media'' by the sentence ''The effect of fluoride contents on the cell viability in culture media after 2 days and 5 days has been presented in Fig. 9. As is evident from the optical microscope images (Fig. 9a) as well as through CCK assay (Fig. 9b), cell viability decreases with increasing fluoride content in glasses. However, the ALP activity of MSCs appeared to increase with increasing fluoride content in glasses as shown in Fig. 9c, thus depicting that fluoride incorporation in glasses did not adversely affect the osteogenic process of rat MSCs under the supply of osteogenic medium.

### 3.4 Chemical dissolution of glasses in aqueous solutions

**3.4.1 Dissolution behavior of glasses in deionized water.** The dissolution of glass powders in DI water for durations varying between 1–120 h did not result in any structural changes or formation of crystalline phases on surface of glasses as is evident from FTIR and XRD data (not shown). However, we did obtain some insight into the impact of fluoride on dissolution behavior

 

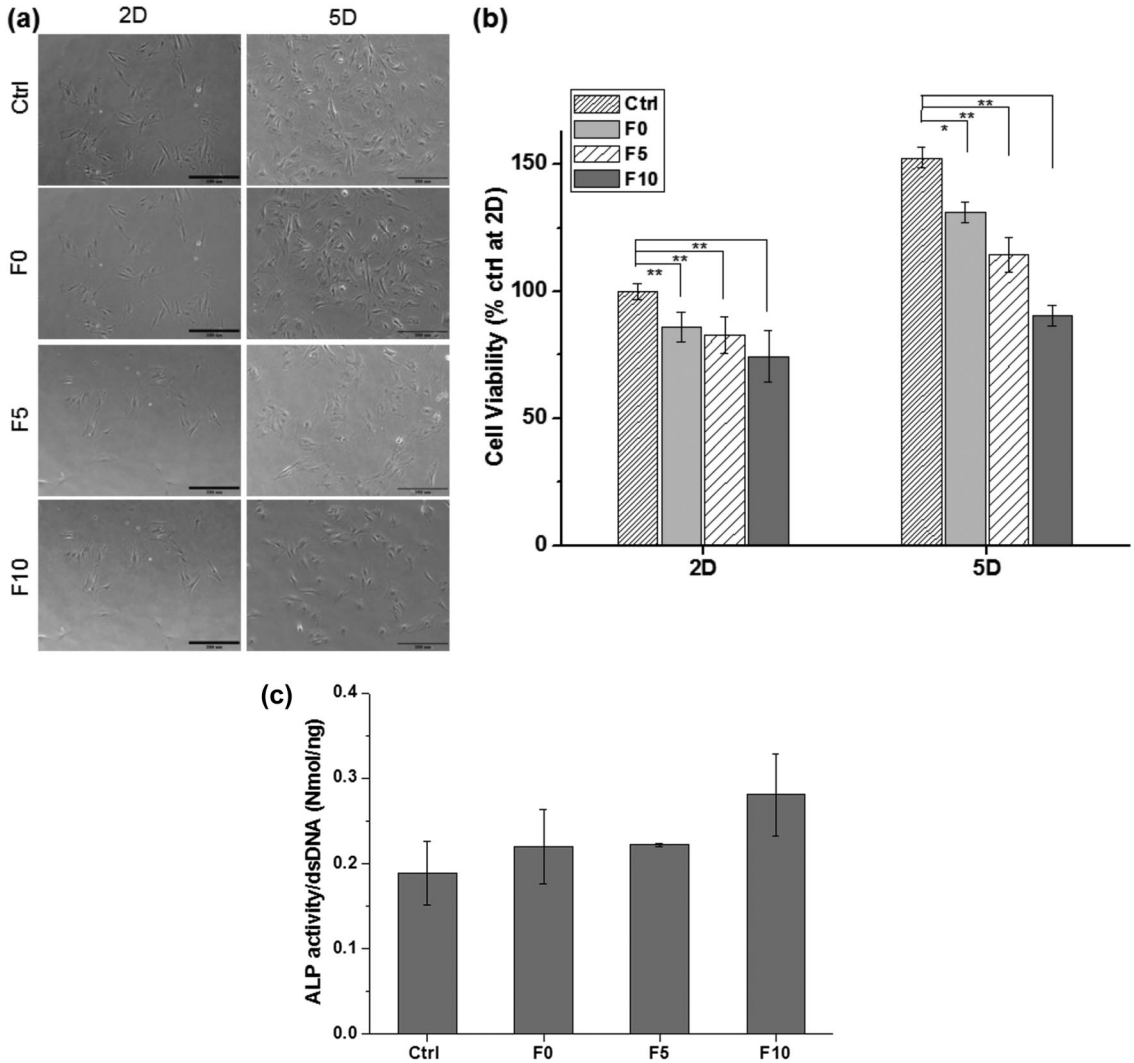


Fig. 9 (a) Cell morphology observed by optical microscopy (scale bar represents 350 μm), and (b) CCK assay of cells, during culture for 2 and 5 days, by means of an indirect test using a transwell insert. Statistical significance; *$p < 0.05$ and **$p < 0.01$, by one-way ANOVA ($n = 3$), (c) ALP activity of cells showing the osteogenic differentiation affected by the different glass samples, during culture for 10 days. The ALP activity was normalized to the dsDNA content.

of phosphate glasses from the elemental release profile of these glasses in DI water. Fig. 10 presents the variation in pH of DI water due to dissolution of glasses over the period of 168 h.

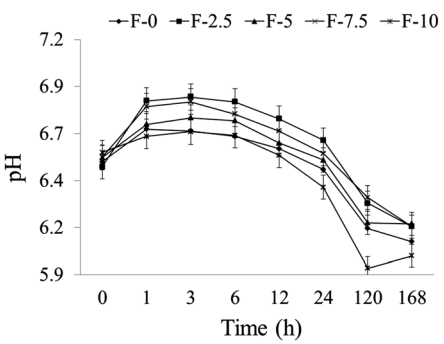


Fig. 10 pH variation of DI water (with time) due to dissolution of glasses.

As expected, the pH values tend to decrease with increasing glass soaking time indicating breakage of P–O–P bonds between the [$PO_4$] units under the attack of $H^+$ ions and molecular water.[56] Since the network breakage reaction is highly sensitive to the attack of $H^+$ ions, decreasing the pH value of aqueous media can further enhance the dissolution rate of these glasses. Fig. 11 presents the normalized sodium release profile of glasses F-0 (Fig. 11a), F-2.5 (Fig. 11b), F-5 (Fig. 11c) and F-7.5 (Fig. 11d) in DI water over the period of 120 h. As is evident from Fig. 11a, the $CaF_2$-free parent glass exhibits forward dissolution rate during initial 3 h after which solution feedback effects could be observed. However, the incorporation of 2.5 mol% $CaF_2$ in glasses prolonged the forward dissolution rate of glasses to 24 h (Fig. 11b). Further increase in $CaF_2$ content ($>2.5$ mol%) in glasses did not affect the dissolution behavior as can be seen in Fig. 11c and d. This increase in duration for forward dissolution rate of glasses from 3 h to 24 h may be attributed to their slower chemical

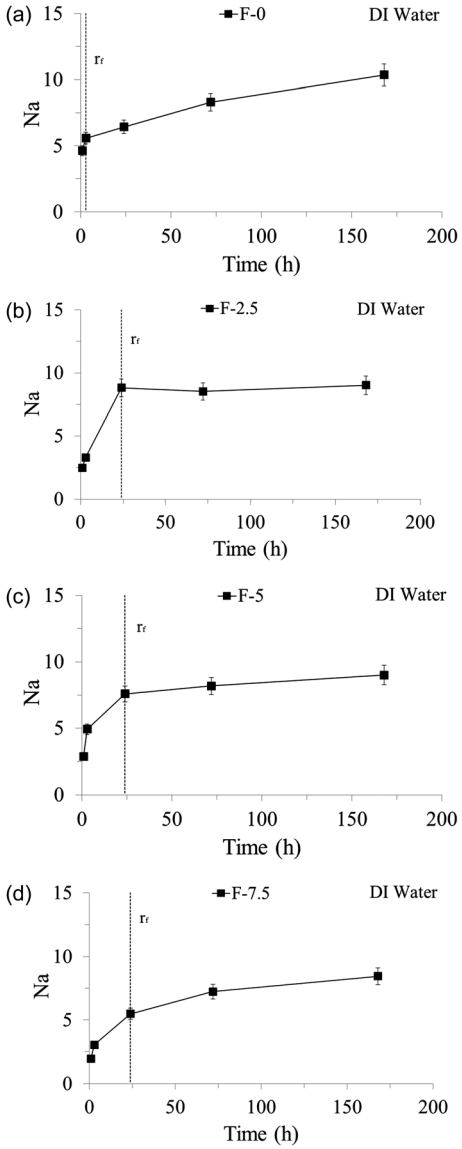


Fig. 11 Normalized sodium release profile of glasses (a) F-0, (b) F-2.5, (c) F-5, (d) F-7.5 after soaking in DI water.

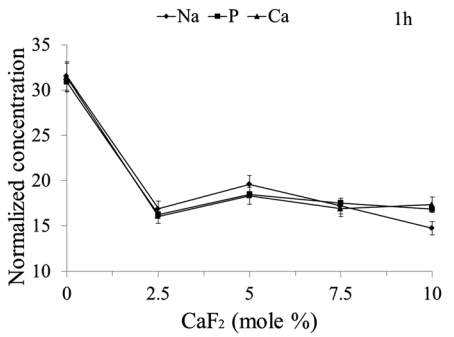


Fig. 12 Normalized release profiles for sodium, calcium and phosphate from glasses (as a function of $CaF_2$ content) after soaking in DI water for 1 h.

degradation under the influence of fluoride content. Fig. 12 presents the normalized release profiles for sodium, calcium and phosphate (as a function of $CaF_2$ content) from glasses in DI water after soaking for 1 h. As is evident from the ICP-OES data, the elemental release from glasses reduces to half (approximately) due to incorporation of 2.5 mol% $CaF_2$. Further increase in $CaF_2$ content did not exhibit significant influence on the dissolution behavior of glasses. These results are in good agreement with the sodium release profile obtained in SBF (Fig. 8) and confirms that fluoride tends to slow down the chemical dissolution of phosphate glasses but only until the stage where glass network structure is not broken by the attack of $H^+$ and molecular water.

**3.4.2 Influence of pH on chemical degradation of glasses.** Fig. 13 presents the weight loss (%) data of glasses (at different pH) as function of their $CaF_2$ content. As is evident from the weight loss data, solution pH had a significant impact on the dissolution behavior of glasses. While phosphate glasses showed significant weight loss (40–50%) in citric acid buffer (pH = 3) over the period of 5 days, increase in solution pH to 7.4 and 9 resulted in tremendous weight gain in glass powders which increased with increasing solution pH. Fluoride incorporation in glasses did not exhibit any significant impact on the trend of the observed weight loss in acidic media. However, an almost linear relationship was observed between weight gain and fluoride content in glasses at pH = 7.4 and 9, where increasing $CaF_2$ content in glasses increased their weight gain.

# 4. Discussion

The chemical dissolution of glasses is a complex topic and there is still no complete consensus on the basic mechanism of glass corrosion that applies to a wide composition space. In particular for phosphate-based bioactive glasses, our understanding of their chemical dissolution has advanced from simple composition-dependent models[56,62–64] to those based on composition–structure–property relationships.[26,60] This evolution has been driven by the idea that the understanding of relationships between chemical composition of glasses and their structure at atomistic level will help us in unearthing the fundamental mechanisms of glass corrosion. This understanding of structure–property relationships in bioactive glasses is of utmost importance for the development of a new generation of gene-activating bioactive glasses with controlled release of functional ions tailored for the treatment of specific conditions.[14] However, despite the ongoing strenuous efforts in this direction,[65] we are still not in a position to develop scientifically robust and statistically accurate models to predict the chemical dissolution behavior of glasses based on their structure–property relationships. This may be attributed to the fact that during dissolution of glasses in aqueous solutions, several chemical processes occur simultaneously within the glass and in solution, so that a rigorous combination of theoretical and experimental studies is required for robust interpretation and reliable predictions of glass corrosion. With this perspective, the present study aims at combining the strengths of experimental and computational studies to elucidate the structural role of fluoride on the chemical dissolution and bioactivity of phosphate based bioactive glasses.

 

It is well known that incorporation of modifier cations ($Ca^{2+}$ and $Na^{+}$) in the phosphate glass network results in the breaking of P–O–P linkages leading to the formation of NBOs, and decrease in their chemical durability.[66] While the two cations compete to bond with the NBOs present in the network, the coordination of Ca is satisfied preferentially over Na, owing to its higher field strength.[60] Similar results have been obtained in the present study through MD simulations, which showed that fluoride tends to associate preferentially with calcium due to the higher ionic field strength of the latter, resulting in the formation of alkali/alkaline-earth rich ionic aggregates ($CaF^{+}$ and, in lower amounts, Na–F) as has also been reported for fluoride containing silicate glasses.[4,43,67] The models highlight that only a minor fraction of fluoride ions are bonded to P for the compositions investigated, even though this P-bonded fraction appears to increase with the $CaF_2$ amount. Nonetheless, the preferential fluoride interaction for these glasses appears to involve the modifier cations. The ability of fluoride ions to strip modifier cations from the glass network induces re-polymerization in the glass structure, thus increasing the network connectivity and slowing down the rate of chemical dissolution. The MD simulation results in this respect are in good agreement with the structural data obtained from $^{31}P$ and $^{23}Na$ MAS-NMR spectroscopy, for which slight re-polymerization in glass structure is evident at higher fluoride content (Table 2). However, unlike the MD simulations, where influence of fluoride on the structure of glasses was evident starting from initial glass composition, in the experimental glasses these structural changes were apparent only at higher $CaF_2$ concentrations, probably due to the partial loss of fluoride from the glasses during melting.

With respect to the apatite forming ability and corrosion of glasses, fluoride incorporation in glasses slows down their chemical dissolution in DI water due to repolymerization of the phosphate glass network, but only until the stage where glass network structure is not broken by the attack of $H^{+}$ and molecular water. However, this increase in chemical durability does not seem to affect their apatite forming ability (in SBF) due to higher solubility (in comparison to silicate glasses) and congruent dissolution behavior of phosphate glasses.

When investigating the influence of pH on the dissolution of phosphate glasses, it has been experimentally shown by Bunker *et al.*[64] that at pH $< 6.5$ (*i.e.* acidic media), phosphate glasses adsorb an excess of protons while at pH $> 6.5$ (neutral and basic media), excess of OH ions are adsorbed. Accordingly, in acidic media, phosphate chains are protonated due to ion exchange reactions between $Na^{+} \leftrightarrow H^{+}$ at the beginning of the glass corrosion process, which disrupts the ionic crosslinks between phosphate chains. This allows water to penetrate into the glass faster, leading to rapid chain hydration and uniform dissolution. Therefore, we could not observe any significant impact of fluoride content on the dissolution of glasses in acidic media as is evident from Fig. 13. However, in basic solutions, it seems that along with OH adsorption, there also exists an ion exchange reaction between $F^{-} \leftrightarrow OH^{-}$ leading to increase in weight with increasing fluoride content (as is evident from Fig. 13). In-depth structural (for example, secondary ion mass spectroscopy, double resonance NMR) and chemical dissolution studies on glass samples are required in order to validate this hypothesis.

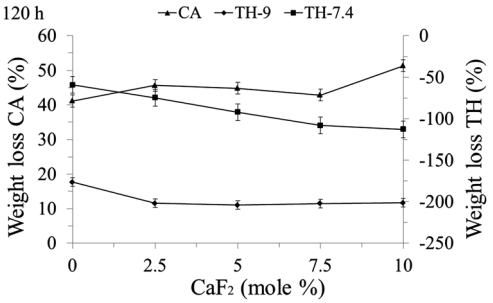


Fig. 13 Weight loss of glass powders (particle size: 300–425 μm), as a function of $CaF_2$ content, after soaking for 120 h in citric acid buffer (pH = 3), tris-HCl (pH = 7.4), and tris-HCl (pH = 9), respectively. Labels TH and CA refer to tris-HCl and citric acid buffer.

## 5. Conclusions

The influence of fluoride on the structure and chemical dissolution behavior of phosphate-based bioactive glasses has been studied. The incorporation of fluoride ions in these glasses induces re-polymerization in the phosphate glass network by stripping the network modifying cations from the glass network. This leads to a slow down of the chemical dissolution of glasses, but only until the stage where the glass network structure is not broken by the attack of $H^{+}$ and molecular water. After this stage, phosphate glasses degrade congruently and fluoride content ceases to have an impact on chemical durability. Due to this reason, no significant influence of fluoride incorporation on the apatite-forming ability of these glasses was detected. However, marked influence of fluoride release from glasses could be observed on cell viability. Therefore, it appears possible to incorporate the beneficial properties of fluoride ions in phosphate-based bioactive glasses without any deterioration in their bioactivity. It is emphasized that volatilization of fluoride from the glass melts needs to be studied further in order to develop a better and precise understanding of structure–property relationships in these glasses. Future research is also warranted on glasses with higher fluoride content, in order to clarify whether the structural trends highlighted here may change when sufficiently high F amounts are incorporated.

## Acknowledgements

The financial support from Rutgers – School of Engineering and Corning Incorporated is acknowledged. A. T. thanks the UK's Royal Society for financial support (RS-URF). This study was also supported in part by the grant from the Global Research Laboratory (GRL; 2015032163) Program, National Research Foundation, Republic of Korea. We also thank Carrie Hogue (Corning) for assistance with some of the NMR measurements, and Shawn Ward (Rutgers) and Sean Langan (Rutgers) for assistance with acquiring Raman spectra of glass powders.

## References


1 A. Wiegand, W. Buchalla and T. Attin, *Dent. Mater.*, 2007, **23**, 343–362.
2 M. A. S. Melo, W. A. Morais, V. F. Passos, J. P. M. Lima and L. K. A. Rodrigues, *Clin. Oral Investig.*, 2014, **18**, 1343–1350.
3 L. G. Petersson, *Clin. Oral Investig.*, 2013, **17**(suppl 1), S63–S71.
4 G. Lusvardi, G. Malavasi, M. Cortada, L. Menabue, M. C. Menziani, A. Pedone and U. Segre, *J. Phys. Chem. B*, 2008, **112**, 12730–12739.
5 I. Kansal, A. Goel, D. U. Tulyaganov, L. F. Santos and J. M. F. Ferreira, *J. Mater. Chem.*, 2011, **21**, 8074–8084.
6 R. V. Law, R. G. H. D. S. Brauer and N. Karpukhina, *J. Mater. Chem*, 2009, **18**, 5629–5636.
7 D. S. Brauer, N. Karpukhina, M. D. O'Donnell, R. V Law and R. G. Hill, *Acta Biomater.*, 2010, **6**, 3275–3282.
8 E. S. Tadjoedin, G. L. de Lange, D. M. Lyaruu, L. Kuiper and E. H. Burger, *Clin. Oral Implants Res.*, 2002, **13**, 428–436.
9 P. P. Cortez, A. F. Brito, S. Kapoor, A. F. Correia, L. M. Atayde, P. Dias-Perreira, A. C. Mauricio, A. Afonso, A. Goel and J. M. F. Ferreira, *J. Biomed. Mater. Res. Part B*, 2015, DOI: 10.1002/jbm.b.33529.
10 L. Bergandi, V. Aina, S. Garetto, G. Malavasi, E. Aldieri, E. Laurenti, L. Matera, C. Morterra and D. Ghigo, *Chem.-Biol. Interact.*, 2010, **183**, 405–415.
11 E. A. Abou Neel, D. M. Pickup, S. P. Valappil, R. J. Newport and J. C. Knowles, *J. Mater. Chem.*, 2009, **19**, 690–701.
12 I. Ahmed, M. Lewis, I. Olsen and J. C. Knowles, *Biomaterials*, 2004, **25**, 491–499.
13 I. Ahmed, M. Lewis, I. Olsen and J. C. Knowles, *Biomaterials*, 2004, **25**, 501–507.
14 K. Franks, I. Abrahams and J. C. Knowles, *J. Mater. Sci.: Mater. Med.*, 2000, **11**, 609–614.
15 V. Salih, K. Franks, M. James, G. W. Hastings, J. C. Knowles and I. Olsen, *J. Mater. Sci.: Mater. Med.*, 2000, **11**, 615–620.
16 M. Bitar, V. Salih, V. Mudera, J. C. Knowles and M. P. Lewis, *Biomaterials*, 2004, **25**, 2283–2292.
17 J. E. Gough, P. Christian, C. A. Scotchford, C. D. Rudd and I. A. Jones, *J. Biomed. Mater. Res.*, 2002, **59**, 481–489.
18 J. E. Gough, P. Christian, C. A. Scotchford and I. A. Jones, *J. Biomed. Mater. Res., Part A*, 2003, **66**, 233–240.
19 D. M. Pickup, E. A. A. Neel, R. M. Moss, K. M. Wetherall, P. Guerry, M. E. Smith, J. C. Knowles and R. J. Newport, *J. Mater. Sci.: Mater. Med.*, Springer, New York LLC, 2008, vol. 19, pp. 1681–1685.
20 R. K. Brow, Z. A. Osborne and R. J. Kirkpatrick, *J. Mater. Res.*, 1992, **7**, 1892–1899.
21 R. K. Brow, C. C. Phifer, X. J. Xu and D. E. Day, *Phys. Chem. Glasses*, 1992, **33**, 33–39.
22 R. K. Brow and Z. A. Osborne, *Surf. Interface Anal.*, 1996, **24**, 91–94.
23 L. F. Santos, R. M. Almeida, V. K. Tikhomirov and A. Jha, *J. Non-Cryst. Solids*, 2001, **284**, 43–48.
24 R. N. D. Karmakar and B. P. Kundu, *Mater. Lett.*, 2002, **57**, 953–958.
25 L. Zhang, C. C. de Araujo and H. Eckert, *J. Phys. Chem. B*, 2007, **111**, 10402–10412.
26 N. H. de L. Jamieson, K. Christie and R. I. Ainsworth, *Biomaterials*, 2014, **35**, 6164–6171.
27 A. Tilocca, *Phys. Chem. Chem. Phys.*, 2014, **16**, 3874–3880.
28 A. Tilocca and A. N. Cormack, *ACS Appl. Mater. Interfaces*, 2009, **1**, 1324–1333.
29 F. Amoureux, J. Huguenard, C. Engelke and F. Taulelle, *Chem. Phys. Lett.*, 2002, **356**, 497–504.
30 W. Smith and T. R. Forester, *J. Mol. Graphics*, 1996, **14**, 136–141.
31 S. Kapoor, A. Goel, A. Tilocca, V. Dhuna, G. Bhatia, K. Dhuna and J. M. F. Ferreira, *Acta Biomater.*, 2014, **10**, 3264–3278.
32 A. Tilocca, *J. Mater. Chem.*, 2010, **20**, 6848–6858.
33 A. Tilocca, *J. Chem. Phys.*, 2008, **129**, 84504.
34 A. Tilocca, N. H. de Leeuw and A. N. Cormack, *Phys. Rev. B: Condens. Matter Mater. Phys.*, 2006, **73**, 104209.
35 A. Tilocca, A. N. Cormack and N. H. de Leeuw, *Chem. Mater.*, 2007, **19**, 95–103.
36 A. Tilocca, A. N. Cormack and N. H. de Leeuw, *Faraday Discuss.*, 2007, **136**, 23–45.
37 G. Lusvardi, G. Malavasi, F. Tarsitano, L. Menabue, M. C. Menziani and A. Pedone, *J. Phys. Chem. B*, 2009, **113**, 10331–10338.
38 A. Tilocca, *J. Chem. Phys.*, 2013, **139**, 114501.
39 A. C. Tas, *Biomaterials*, 2000, **21**, 1429–1438.
40 D. S. Brauer, M. Mneimne and R. G. Hill, *J. Non-Cryst. Solids*, 2011, **357**, 3328–3333.
41 A. Hrubý, *Czech. J. Phys. B*, 1972, **22**, 1187–1193.
42 D. Carta, D. M. Pickup, J. C. Knowles, I. Ahmed, M. E. Smith and R. J. Newport, *J. Non-Cryst. Solids*, 2007, **353**, 1759–1765.
43 J. K. Christie, A. Pedone, M. C. Menziani and A. Tilocca, *J. Phys. Chem. B*, 2011, **115**, 2038–2045.
44 A. Pedone, T. Charpentier and M. C. Menziani, *J. Mater. Chem.*, 2012, **22**, 12599–12608.
45 R. I. Ainsworth, D. Di Tommaso, J. K. Christie and N. H. de Leeuw, *J. Chem. Phys.*, 2012, **137**, 234502.
46 D. Ilieva, B. Jivov, G. Bogachev, C. Petkov, I. Penkov and Y. Dimitriev, *J. Non-Cryst. Solids*, 2001, **283**, 195–202.
47 P. Y. Shih, S. W. Yung and T. S. Chin, *J. Non-Cryst. Solids*, 1999, **244**, 211–222.
48 A. F. Lemos, J. H. G. Rocha, S. S. F. Quaresma, S. Kannan, F. N. Oktar, S. Agathopoulos and J. M. F. Ferreira, *J. Eur. Ceram. Soc.*, 2006, **26**, 3639–3646.
49 H. Tsuda and J. Arends, *J. Dent. Res.*, 1994, **73**, 1703–1710.
50 S. Amini, A. Masic, L. Bertinetti, J. S. Teguh, J. S. Herrin, X. Zhu, H. Su and A. Miserez, *Nat. Commun.*, 2014, **5**, 3187.
51 A. Aminzadeh, M. Meskinfam and S. F. Tayyary, *Spectrochim. Acta, Part A*, 2007, **66**, 199–201.
52 A. Aminzadeh, *Spectrochim. Acta, Part A*, 1997, **53**, 693–697.
53 E. Landi, G. Celotti, G. Logroscino and A. Tampieri, *J. Eur. Ceram. Soc.*, 2003, **23**, 2931–2937.
54 H. H. Alder and P. F. Kerr, *Am. Mineral.*, 1962, **47**, 700–717.
55 C. Rey, B. Collins, T. Goehl, I. R. Dickson and M. J. Glimcher, *Calcif. Tissue Int.*, 1989, **45**, 157–164.
56 H. Gao, T. Tan and D. Wang, *J. Controlled Release*, 2004, **96**, 29–36.


 

57 J. Massera, K. Bourhis, L. Petit, M. Couzi, L. Hupa, M. Hupa, J. J. Videau and T. Cardinal, *J. Phys. Chem. Solids*, 2013, **74**, 121–127.
58 F. Dohler, A. Mandlule, L. van Wullen, M. Friedrich and D. S. Brauer, *J. Mater. Chem. B*, 2015, **3**, 1125–1134.
59 M. R. Filgueiras, G. LaTorre and L. L. Hench, *J. Biomed. Mater. Res.*, 1993, **27**, 1485–1493.
60 J. K. Christie, R. I. Ainsworth, D. Di Tommaso and N. H. de Leeuw, *J. Phys. Chem. B*, 2013, **117**, 10652–10657.
61 G. Lusvardi, G. Malavasi, L. Menabue, V. Aina and C. Morterra, *Acta Biomater.*, 2009, **5**, 3548–3562.
62 M. Ogino, F. Ohuchi and L. L. Hench, *J. Biomed. Mater. Res.*, 1980, **14**, 55–64.
63 S. F. Khor, Z. A. Talib, W. M. Daud and H. A. A. Sidek, *J. Mater. Sci.*, 2011, **46**, 7895–7900.
64 B. C. Bunker, G. W. Arnold and J. A. Wilder, *J. Non-Cryst. Solids*, 1984, **64**, 291–316.
65 J. K. Christie and A. Tilocca, *J. Mater. Chem.*, 2012, **22**, 12023–12031.
66 D. M. Pickup, I. Ahmed, J. C. Knowles, M. E. Smith and R. J. Newport, *J. Phys.: Condens. Matter*, 2007, **19**, 415116.
67 J. F. Stebbins and Q. Zeng, *J. Non-Cryst. Solids*, 2000, **262**, 1–5.